Transp Porous Med (2016) 111:591–603
DOI 10.1007/s11242-015-0613-7

Helical Flow and Transient Solute Dilution in Porous Media

Gabriele Chiogna[1,2] · **Olaf A. Cirpka**[1] · **Paulo A. Herrera**[3,4]

Received: 3 June 2015 / Accepted: 7 December 2015 / Published online: 12 December 2015

Abstract Helical flow can occur in porous media if the hydraulic conductivity tensor is anisotropic. We study the structure of steady-state flow fields in three-dimensional anisotropic porous media formed by two homogeneous layers, one of which is anisotropic. We simulate transient transport of a conservative scalar in such flow fields by a hybrid streamline/smoothed particle hydrodynamics method and analyze dilution. We use stretching and folding metrics to characterize the flow field and the dilution index of a conservative scalar divided by the volume of the domain to quantify plume dilution. Based on the results of detailed numerical simulations, we conclude that nonlinear deformation triggers dilution and that plume dilution is controlled by two parameters: the contrast between the principal directions of the anisotropic layer, and the orientation of the hydraulic conductivity tensor with respect to the main flow direction. Furthermore, we show that in this kind of flow fields transverse dispersion is responsible for an increase in plume dilution, while the effect of longitudinal dispersion is negligible.

Keywords Anisotropic porous media · Helical flow · Flow topology · Solute dilution

✉ Paulo A. Herrera
paulo.herrera.ricci@gmail.com

Gabriele Chiogna
gabriele.chiogna@uni-tuebingen.de

Olaf A. Cirpka
olaf.cirpka@uni-tuebingen.de

1 Center for Applied Geoscience, University of Tübingen, Hölderlinstr. 12, 72074 Tübingen, Germany

2 Faculty for Civil, Geo and Environmental Engineering, Technical University of Munich, Darcistrasse 21, 80333 Munich, Germany

3 Department of Civil Engineering, University of Chile, Av. Blanco Encalada 2002, 8370449 Santiago, Chile

4 Andean Geothermal Center of Excellence, University of Chile, Plaza Ercilla 803, 8370450 Santiago, Chile

1 Introduction

Mixing processes are important in fluid mechanics due to their relevance for many environmental, engineering, and physical problems (Ottino 1989; Duplay and Sen 2004; Hidalgo et al. 2012). Solute dilution in steady-state flows at low Reynolds number ($Re << 10$), which are typical of many natural and engineered porous media, chemical reactors, and microchannels, is in general poor and controlled by slow diffusive processes. It strongly depends on the structure of the flow field (Rolle et al. 2012; Stroock et al. 2002; Higler et al. 1999; van Baten et al. 2001) and on its capability of generating concentration gradients. Among other approaches, some recent studies aimed at describing mixing and mixing-controlled processes in two-dimensional porous media, investigated and characterized topological (de Barros et al. 2012) and kinematic (Le Borgne et al. 2013) features of the flow field, to understand and quantify the dependence of dilution on the flow structure.

Three-dimensional flow fields can display additional mixing enhancement mechanisms such as the occurrence of secondary helical motion (Holm and Kimura 1991; Moffatt 2014; Stroock et al. 2002; Villermaux et al. 2008; Toussaint et al. 1995). While flow in stationary heterogeneous isotropic porous media is constrained on Lamb surfaces (Sposito 1994, 2001) and its impact on solute transport has been widely investigated in the past decades, the impact of complex (e.g., helical) steady-state flow configurations that can occur in anisotropic porous media has not been investigated in detail. In anisotropic porous media, streamlines are not necessarily perpendicular to equipotential surfaces (Bear 1972), and the solution of Darcy's law may lead to the definition of three-dimensional steady-state flow fields, which may exhibit nonzero helicity density, i.e., the scalar product between the velocity and its vorticity (Moffatt and Tsinober 1992; Chiogna et al. 2014). Therefore, helical flow can occur in this type of media (Ye et al. 2015). Notice that, contrary to Stokes flows, Darcy flows are helical only if appropriate boundary conditions are applied and the anisotropy of the porous medium is preserved during upscaling (Chiogna et al. 2014). Hence, the solution of Darcy's law admits the occurrence of scale-dependent helical flows in porous media, even if they are composed by simple homogeneous anisotropic blocks (Chiogna et al. 2015; Bakker and Hemker 2004; Hemker et al. 2004; Hemker and Bakker 2006; Stauffer 2007; Ginzburg and dHumires 2007). Cirpka et al. (2015) have shown that under steady-state transport conditions twisting streamlines are the main source of plume deformation controlling mixing enhancement.

The main purpose of this manuscript is to investigate how helical flows in anisotropic porous media affect transient solute transport at the continuum scale and how mixing depends on the anisotropy of the hydraulic conductivity tensor. This is particularly relevant for the construction of engineered mixing devices, for natural locally anisotropic porous media (Koza et al. 2009; Matyca et al. 2013; Hsieh et al. 1985; Gao et al. 2012), and also for flows at scales typical of geological structures (i.e., tens of meters).

2 Mathematical Formulation

2.1 Flow in Porous Media

The distinctive aspect of investigating flow and transport in porous media is the complex interplay between processes occurring at multiple spatial scales (Rolle et al. 2013; Hyman and Winter 2013). It has recently been shown that Stokes flow, which describes flow within individual pores, can cause chaotic advection if the pore geometry is sufficiently complex.

This can greatly enhance mixing on that scale (Lester et al. 2013). Yet, for applications in the fields of hydrogeology and chemical engineering, pore-scale processes are upscaled, and the porous medium is considered a continuum. In this work, we will consider flow and transport on the continuum scale (involving at least several hundred pores). At this scale, and for $Re << 10$, flow of an incompressible fluid is well described by Darcy's law:

$$\mathbf{v} = -\frac{\mathbf{k}\rho g}{n\mu}\nabla\left(z + \frac{p}{\rho g}\right) \tag{1}$$

where $\mathbf{v}$ is the average pore flow velocity, n is the effective porosity, $\mathbf{k}$ is the intrinsic permeability, μ is the viscosity, ρ is the density of the fluid, p is the fluid pressure, and z is the spatial coordinate parallel to gravity. For the case of water flow, the average pore water velocity is usually expressed in terms of the hydraulic conductivity $\mathbf{K}$ and the hydraulic head ϕ, $\mathbf{v} = -\frac{\mathbf{K}}{n}\nabla\phi$, with $\phi = \frac{p}{\rho g} + z$.

Spatially variable velocity fields at the continuum scale are typical for natural and engineered porous media, mainly due to the heterogeneity of the hydraulic conductivity tensor $\mathbf{K}$. They induce deformation of a solute plume, enhancing concentration gradients that counteract the smoothing effect of diffusion (Le Borgne et al. 2010, 2015), which has been extensively studied in the literature.

At the continuum or Darcy scale, the hydraulic conductivity is a full tensor as result of local anisotropy in the pore network (e.g., Kim et al. 1987; Pilotti 1998) and depends on the tortuosity of the pore-scale flow paths (Bear 1972; Guo 2012). At scales typical of field scale investigations, the structure of the geological heterogeneity remains widely unknown. Full hydraulic conductivity tensors may be required to parametrize the anisotropic heterogeneity of natural porous media (e.g., Hsieh et al. 1985; Indelman and Dagan 1993). This is a typical situation encountered in hydrogeology (e.g., Neuman et al. 1984; Hsieh et al. 1985).

2.2 The Bakker and Hemker's Flow Field

In this study, we will consider the multilayered semi-analytical solution of the flow velocity components by Bakker and Hemker (2004). This solution has been validated by detailed numerical simulations (Bakker and Hemker 2004). We investigate this particular set up, because it is probably the simplest in which helical flow may arise in porous media. The solution assumes no-flow boundary conditions at boundaries orthogonal to the y and z axes, i.e., top, bottom, left, and right sides, of a three-dimensional domain of width $2d$ and height $2H$ as shown in Fig. 1. The flow in the x direction is driven by a constant hydraulic gradient σ. The medium is composed by an upper homogeneous anisotropic layer (layer 1) with hydraulic conductivity $\mathbf{K}_1$ and a lower homogeneous isotropic layer (layer 2) with hydraulic conductivity $\mathbf{K}_2$ of the same thickness H and porosity n. While the homogeneous isotropic hydraulic conductivity tensor of the lower layer is invariant upon rotation, the principal directions $K_{\tilde{x}\tilde{x},1}$, $K_{\tilde{y}\tilde{y},1}$, and $K_{\tilde{z}\tilde{z},1}$ of the anisotropic tensor in the upper layer may have an orientation differing from the mean velocity field. We will consider the tensor rotated only in the x–y plane, such that it forms an angle β with the positive y axis. The following relations hold:

$$K_{xx,1} = K_{\tilde{x}\tilde{x},1}\sin^2\beta + K_{\tilde{y}\tilde{y},1}\cos^2\beta \tag{2}$$

$$K_{yy,1} = K_{\tilde{y}\tilde{y},1}\sin^2\beta + K_{\tilde{x}\tilde{x},1}\cos^2\beta \tag{3}$$

$$K_{xy,1} = \left(K_{\tilde{x}\tilde{x},1} - K_{\tilde{y}\tilde{y},1}\right)\sin^2\beta\cos^2\beta \tag{4}$$

$$K_{zz,1} = K_{\tilde{z}\tilde{z},1} \tag{5}$$

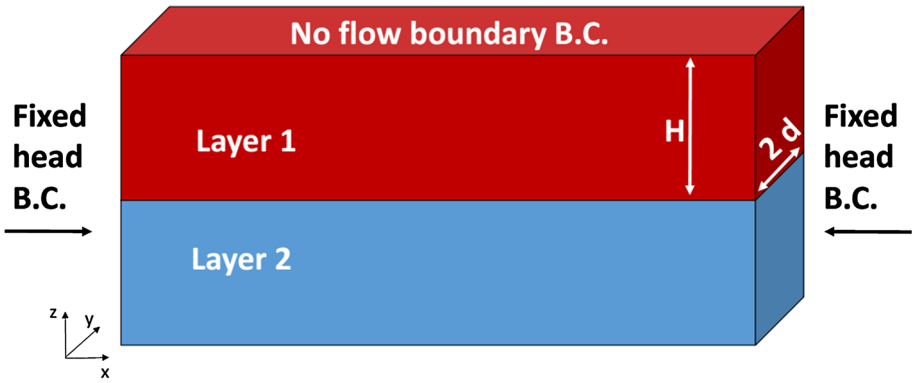

Fig. 1 Schematic representation of the two-layer domain considered in the numerical simulations

The components of the velocity field in the x- and y-direction for layer 1 read as:

$$v_{x,1} = -\left(\frac{K_{xy,1}}{K_{yy,1}+K_{yy,2}}\left[K_{xy,1}+K_{xy,2}\right.\right.$$
$$\left.\left.+K_{yy,2}\left(\frac{K_{xy,1}}{K_{yy,1}}-\frac{K_{xy,2}}{K_{yy,2}}\right)\frac{\cosh(y/\lambda)}{\cosh(d/\lambda)}\right]+K_{xx,1}\right)\frac{\sigma}{n} \tag{6}$$

$$v_{y,1} = \frac{K_{xy,1}K_{yy,2}-K_{xy,2}K_{yy,1}}{K_{yy,1}+K_{yy,2}}\left(1-\frac{\cosh(y/\lambda)}{\cosh(d/\lambda)}\right)\frac{\sigma}{n} \tag{7}$$

and for layer 2 as:

$$v_{x,2} = -\left(\frac{K_{xy,2}}{K_{yy,1}+K_{yy,2}}\left[K_{xy,1}+K_{xy,2}\right.\right.$$
$$\left.\left.-K_{yy,1}\left(\frac{K_{xy,1}}{K_{yy,1}}-\frac{K_{xy,2}}{K_{yy,2}}\right)\frac{\cosh(y/\lambda)}{\cosh(d/\lambda)}\right]+K_{xx,2}\right)\frac{\sigma}{n} \tag{8}$$

$$v_{y,2} = -\frac{K_{xy,1}K_{yy,2}-K_{xy,2}K_{yy,1}}{K_{yy,1}+K_{yy,2}}\left(1-\frac{\cosh(y/\lambda)}{\cosh(d/\lambda)}\right)\frac{\sigma}{n} \tag{9}$$

while the flow velocity at the interface between the two layers is given by

$$v_z = \frac{-\sigma\lambda}{\hat{c}n\left(K_{yy,1}+K_{yy,2}\right)}\frac{\sinh(x/\lambda)}{\cosh(d/\lambda)}\left(\frac{K_{xy,1}}{K_{yy,1}}-\frac{K_{xy,2}}{K_{yy,2}}\right)\left(K_{yy,1}-K_{yy,2}\right) \tag{10}$$

where

$$\lambda = \sqrt{\frac{\hat{c}K_{yy,2}K_{yy,1}}{K_{yy,2}+K_{yy,1}}} \tag{11}$$

and

$$\hat{c} = \frac{H}{2}\frac{K_{zz,1}+K_{zz,2}}{K_{zz,1}K_{zz,2}} \tag{12}$$

Differently from other studies focusing on mixing processes in porous media, the spatial variability of the flow field under investigation is not controlled by shearing driven by a spatially random hydraulic conductivity, but by the angle β of the anisotropy orientation and the anisotropy ratio $R = K_{\tilde{x}\tilde{x},1}/K_{\tilde{y}\tilde{y},1}$. Figure 2 shows that the flow field varies along the

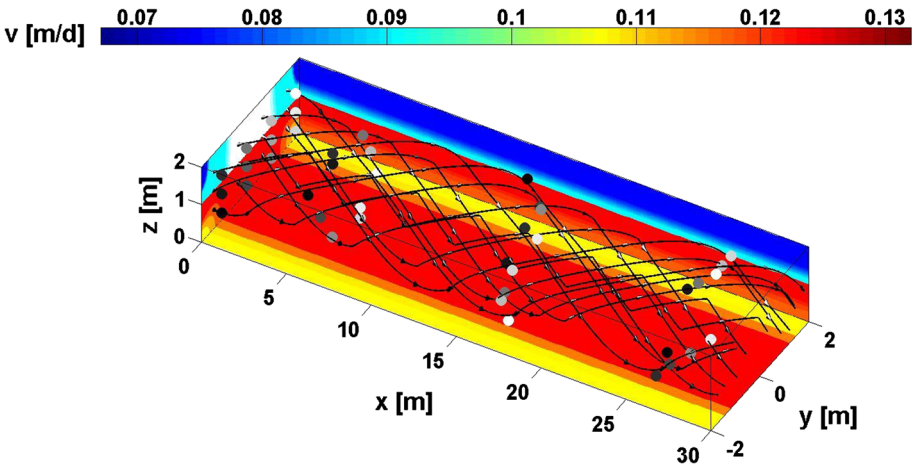

Fig. 2 Streamlines and position of advected particles at four different time steps. *Colorbar* refers to the module of the flow velocity

Table 1 Parameters characterizing the flow fields: $\langle v_x \rangle$ is the mean flow velocity in the x direction and β, R, $K_{xx,1}$, $K_{yy,1}$, $K_{zz,1}$, $K_{xy,1}$, $K_{xx,2}$, $K_{yy,2}$, $K_{zz,2}$, and $K_{xy,2}$ refer to the properties of the hydraulic conductivity tensors of layers 1 and 2

$\langle v_x \rangle$	β	R	$K_{xx,1}$	$K_{yy,1}$	$K_{zz,1}$	$K_{xy,1}$	$K_{xx,2}$	$K_{yy,2}$	$K_{zz,2}$	$K_{xy,2}$
0.1470	15°	5	9.5	2.5	6	2	6	6	6	0
0.1219	30°	5	8	4	6	3.5	6	6	6	0
0.1188	45°	1.4	6	6	6	1	6	6	6	0
0.1155	45°	2	6	6	6	2	6	6	6	0
0.1098	45°	3	6	6	6	3	6	6	6	0
0.1019	45°	5	6	6	6	4	6	6	6	0

Mean flow velocity and hydraulic conductivity are expressed in m day^{-1}

y- and z-directions, while it does not depend upon the x-direction. Advected particles are affected by shearing in the x-direction, and secondary motion twists the streamlines in the $y-z$ plane. Therefore, the plane formed by a set of particles starting at a given cross section x_0 is deformed by the flow field in all three spatial dimensions, as shown in Fig. 2. In this study, we consider six different flow configurations defined by the parameters summarized in Table 1 with identical values of the hydraulic gradient $\sigma = 0.0017$ and porosity $n = 0.1$.

2.3 Numerical Solution of Solute Transport in Porous Media

Solute transport at the Darcy's scale is described by the conservative advection–dispersion equation:

$$\frac{\partial c}{\partial t} = \mathbf{v} \cdot \nabla c - \nabla \cdot (\mathbf{D} \nabla c) \tag{13}$$

where $\mathbf{D}$ is defined for simplicity as the sum of a pore diffusion term D_p independent on the flow velocity, and a mechanical dispersion term, which depends linearly on the flow velocity and on the dispersivity tensor α (Scheidegger 1961). The components of $\mathbf{D}$ can be

computed as $D_{ij} = \alpha_T|\mathbf{v}| + (\alpha_L - \alpha_T)v_i v_j/|\mathbf{v}|$ (Bear 1972). The effects of pore-scale velocity fluctuations and mixing on continuum-scale solute transport are typically parametrized by this latter term. In this study, we set $D_p = 1.16 \times 10^{-9}$ m^2 s^{-1}, the dispersivity in the longitudinal direction $\alpha_L = 1 \times 10^{-2}$ m, and the dispersivity in the two transverse directions $\alpha_T = 1 \times 10^{-3}$ m.

Equation 13 has been solved numerically using a hybrid streamline smoothed particle hydrodynamics (SPH) method (Herrera et al. 2010). This numerical method has been tested and validated in previous studies against both analytical and other numerical solutions (Herrera et al. 2009, 2010). Solute transport due to advection and longitudinal dispersion is simulated along streamlines, while the effect of transverse dispersion is approximated with a SPH expression for diffusive terms (Cleary and Monaghan 1999), which has been previously used to simulate pore-scale and continuum-scale dispersion in porous media (e.g., Zhu and Fox 2002; Tartakovsky et al. 2008; Herrera et al. 2009). The main advantage of this numerical method is that it completely removes transverse numerical dispersion and that the numerical grid automatically adapts to the flow field. Hence, it is particularly well-suited to investigate the effect of transverse dispersion on transient mixing and dilution in helical flow fields. In this numerical formulation, the accuracy of the solution depends on the discretization along streamlines, which impacts the numerical solution of advection and longitudinal dispersion, and the spacing between streamlines (Herrera et al. 2009), which is important to obtain a good resolution to simulate transverse dispersion. To obtain the results presented below, we first computed a velocity field on a 12-million-cell grid, traced 3200 streamlines, and finally discretized the streamlines with 1.2 million nodes. The total simulated time was 180 days, which was discretized in constant time steps in order to satisfy the stability criteria of the numerical solver. This fine discretization was needed to reproduce the complexity of the flow field and to obtain a high resolution in the transport simulations.

3 Metrics to Characterize Flow Kinematic and Plume Dilution

3.1 Stretching and Folding

To characterize the kinematic properties of the flow field, we compute stretching and folding of solute spheres at different time intervals following the approach of Falk and Langer (1998) and Kelley and Ouellette (2011). This approach allows to separate linear (stretching) from nonlinear (folding) deformation of spherical particle clusters covering the domain of interest. This approach was first introduced to capture the dynamics of viscoplastic deformation in amorphous solids (Falk and Langer 1998) and then applied to characterized two-dimensional turbulent flows (Kelley and Ouellette 2011). In this work, we extend the typical two-dimensional formulation, to a three-dimensional one, since we are interested in quantify the deformation occurring in the complex flow field described by Eqs. 6–10.

Stretching is defined as the squared L_2-norm of the affine deformation of a set of 629 spheres to cover the entire area of the injection plane of the domain. Each sphere has radius $r_0 = 0.05$ and is formed by N particles (where $N = 101$ was selected by trial and error in a convergence study):

$$A^2(\mathbf{x}, \Delta t) = \frac{1}{r_0^2 N} \sum_{n=1}^{N} \left\| \mathbf{A}\mathbf{d}^n(t) \right\|_2^2 \tag{14}$$

Similarly, folding is defined as the squared L_2-norm of the non-affine (nonlinear) part of the overall deformation:

$$D^2(\mathbf{x}, \Delta t) = \frac{1}{r_0^2 N} \sum_{n=1}^{N} \left\| \mathbf{d}^n(t + \Delta t) - (\mathbf{A} + \mathbf{I})\, \mathbf{d}^n(t) \right\|_2^2 \tag{15}$$

where $\mathbf{A}$ is the affine deformation matrix computed by least square fitting (Falk and Langer 1998), $\mathbf{I}$ is the identity matrix and $\mathbf{d}$ is the vector of the distances between each particle to the central particle, i.e., the distance for particle i is:

$$\mathbf{d}^i(t) = \mathbf{x}^0(t) - \mathbf{x}^i(t) \tag{16}$$

where $\mathbf{x}^i(t)$ are the spatial coordinates of particle n at time t.

In this framework, folding represents the inability to describe the temporal deformation of the initial sphere with a purely linear model. While stretching represents the increase in the surface of a volume, folding describes how this interface is bent in order to fill a finite volume of space (Kelley and Ouellette 2011).

3.2 Dilution Index

We compute the reactor ratio $M\,[-]$ to quantify the degree of solute dilution (Kitanidis 1994):

$$M(t) = \frac{E(t)}{V}, \tag{17}$$

where V is the volume of the computational domain and $E(t)\ [L^3]$ is the dilution index, defined as the exponential of the Shannon entropy of the scalar concentration:

$$E(t) = \exp\left(- \int_{-\infty}^{+\infty} \int_{-\infty}^{+\infty} \int_{-\infty}^{+\infty} p(x, y, z, t) \ln\left(p(x, y, z, t)\right) \mathrm{d}x\mathrm{d}y\mathrm{d}z \right), \tag{18}$$

in which $p(x, y, z, t)\ [L^{-3}]$ is the density of solute mass in the domain at time t calculated as:

$$p(x, y, z, t) = \frac{c(x, y, z, t)}{\left(\int_{-\infty}^{+\infty} \int_{-\infty}^{+\infty} \int_{-\infty}^{+\infty} c(x', y', z', t) \mathrm{d}x'\mathrm{d}y'\mathrm{d}z' \right)} \tag{19}$$

Thus, $E(t)$ represents the effective volume over which the mass is distributed, which is normalized by its maximum value equal to the total domain volume to obtain $M(t)$.

4 Results and Discussion

4.1 Kinematic Properties of the Flow Fields

Figure 3 represents the complex dynamics of stretching and folding for the flow field computed by Eqs. 6–10. Figure 3a–f shows, for the six cases considered, the logarithm of the ratio between stretching and folding calculated for each sphere at time $t/\tau = 0.65$, with $\tau = L/\langle v_x \rangle$ and $L = 50$ m is the length of the computational domain, projected onto the plane $x = 0$ according to the initial position of the center particle. The deformation is nonlinear for spheres placed close to the discontinuity of the flow field at $z = 1$, due to the sharp change in the magnitude of v_x between the two layers. For all cases, there is a similar distribution of folding dominated spheres that form two spiral arms. The number of

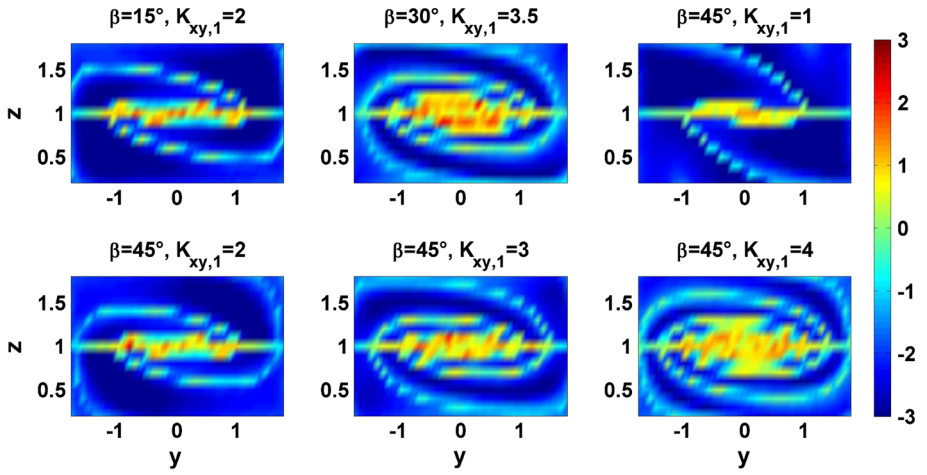

Fig. 3 Evolution of the logarithm of stretching and folding ratios (*colorbar*) projected onto the initial starting plane of the spheres for $t/\tau = 0.65$

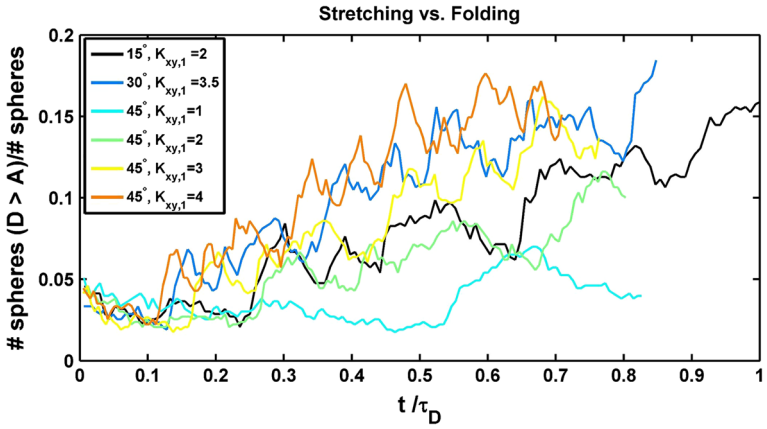

Fig. 4 Fraction of spheres for which folding is greater than stretching as function of time for the six cases considered

nonlinearly deformed spheres increases with time, as shown in Fig. 4. At early times, the number of spheres where folding dominates is similar for all cases, because initially the deformation is controlled by processes occurring at the interface between the two layers. At later times, the nonlinear deformation propagates faster in the y–z plane for higher values of the non-diagonal term $K_{xy,1}$, because in these cases the rotational velocity is higher.

4.2 Mixing Enhancement

Figure 5 presents the time evolution of the reactor ratio for two spheres of radius $r = 0.2$, centered at coordinates (1.0, 0.0, 1.0) and (1.0, 0.0, 1.3), respectively, at time $t = 0$. Figure 5a, b shows results considering a full dispersion tensor, and Fig. 5c, d shows results obtained considering only longitudinal dispersion for four different anisotropy ratios and an angle $\beta = 45°$. Both spheres dilute faster (expressed by a quicker increasing reactor ratio) for

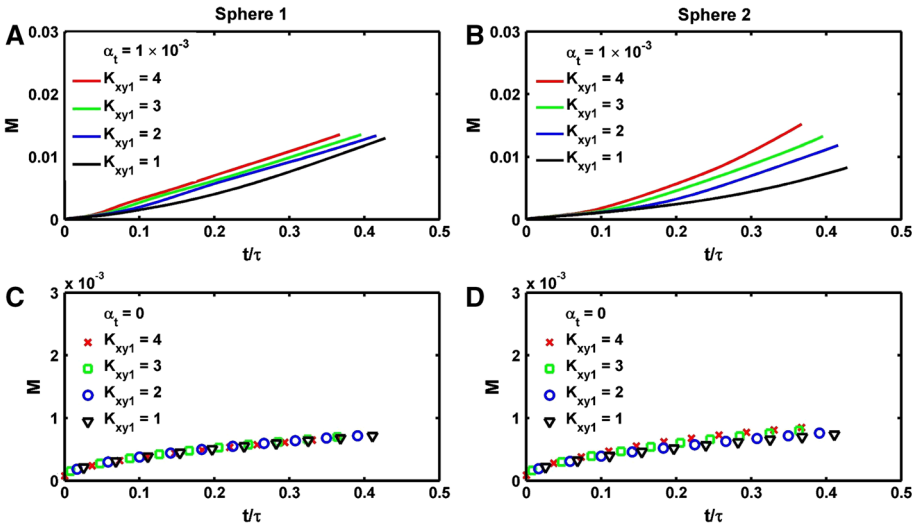

Fig. 5 Reactor ratio for two spheres centered at (1.0, 0.0, 1.0) (**a**) and (1.0, 0.0, 1.3) (**b**) at time $t = 0$ considering four different anisotropy ratios and $\alpha_t = 1 \times 10^{-3}$. The same spheres are considered in **c**, **d**, respectively, considering only longitudinal dispersion (i.e., $D_t = 0$)

larger anisotropy ratio and, hence, larger helicity (Chiogna et al. 2014). Moreover, the initial position of the spheres influences both the rate of increase of M and its magnitude in a complex way. Where the deformation is mainly driven by folding, i.e., sphere 1, the values of the reactor ratio for the different anisotropy ratios do not differ that much among, in particular at late times. However, after a rapid increase in plume deformation which leads to the creation of thinner spiral arms of the plume with a smaller relative distance, diffusion homogenizes the concentration gradients. Then, the effective area where diffusive processes effectively occur decreases more rapidly for sphere 1 than for sphere 2, such that the reactor ratio at late times can become higher for sphere 2 than for sphere 1, e.g., for $K_{xy,1} = 4$. A comparison between Fig. 5a–d, shows that, in the presence of transverse dispersion, dilution is enhanced by the helical shape of the streamlines, while it is not significantly different when dispersion acts only in the longitudinal direction.

Figure 6 shows how the reactor ratio depends on the angle β of the anisotropy orientation. We can observe that, in general, the reactor ratio increases with the angle. However, for sphere 1 the reactor ratio rapidly converges to the same value. In these three cases, the spheres rapidly move in the y–z plane, passing through regions where nonlinear deformations are more or less pronounced. Shearing caused by the difference between the velocity in the x-direction in the two layers is the main deformation process for sphere 1, and this process is common to all three angles considered. This explains the similarity in the dilution index computed for these three cases. In the case of sphere 2, whose deformation is less influenced by shearing in the x-direction since the distance between the starting point of the spheres and the boundary of the two layers is larger, the dilution index decreases according to the orientation angle of the conductivity tensor.

The results obtained for the reactor ratio are in agreement with the analysis of stretching and folding. Dilution is enhanced mainly by folding processes, and the flow field characterized by the fastest helical motion displays both the fastest increase in folding and the fastest increase in the reactor ratio. However, since stretching and folding are global measures of the velocity

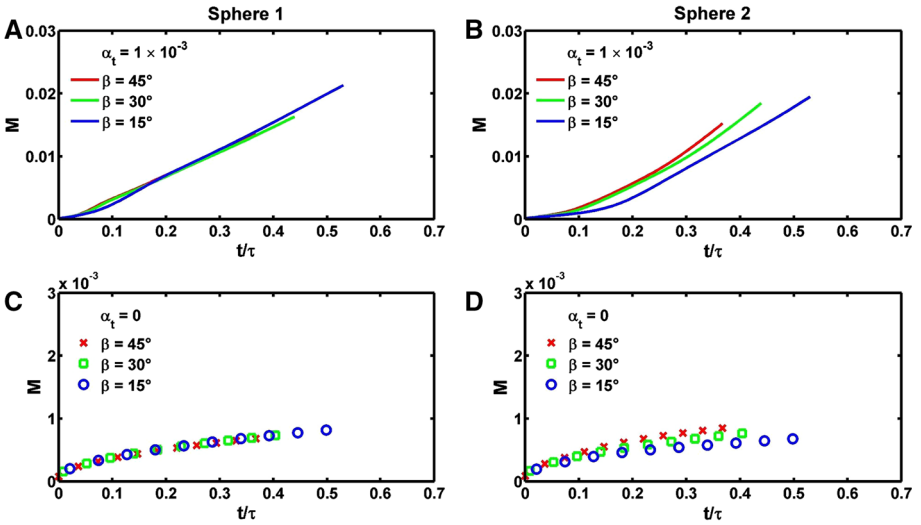

Fig. 6 Reactor ratio for two spheres centered at (1.0, 0.0, 1.0) (**a**) and (1.0, 0.0, 1.3) (**b**) at time $t = 0$ considering three different angles β and $\alpha_t = 1 \times 10^{-3}$. The same spheres are considered in **c**, **d**, respectively, considering only longitudinal dispersion (i.e., $D_t = 0$)

field, they can only provide general information about the efficiency of mixing processes, which can be expected in a given flow field. In addition, they can also be applied to identify the areas where more efficient mixing can occur. On the contrary, the dilution index is specific for each scenario investigated, and it is informative of how well an individual solute plume is diluted. However, its computation requires the evaluation of the spatial distribution of concentration.

The correlation between helical flow and dilution found by Cirpka et al. (2015) for steady-state transport is confirmed by this study also under transient transport conditions. In addition, the results shown in Figs. 5 and 6 show that in this kind of helical flow fields, despite the heterogeneity of the velocity field, longitudinal mixing is not significantly enhanced in comparison with transverse mixing.

The structure of the porous medium investigated in this study is representative for engineered fixed-bed chemical reactors and geologic formation in which an effective hydraulic conductivity tensor is defined. In more complex porous formations, such as natural aquifers, also the intrinsic heterogeneity of the medium will play a significant role for the enhancement of dilution. Yet, this will be an additional effect to the one presented in this work, as shown for steady-state flow and transport conditions by Cirpka et al. (2015) and Chiogna et al. (2015)

5 Conclusions

This work has shown that helical flow occurring in anisotropic porous media at the continuum scale significantly influences dilution of a conservative scalar quantity. The mixing enhancement observed at this scale is complementary to that achieved at the microscopic level (Stroock et al. 2002; Lester et al. 2013), which is parametrized with the aid of the dispersion tensor.

In our study, dilution is controlled by the magnitude of the local dispersion coefficients and two additional parameters: The anisotropy ratio R and the relative angle β between the flow

field and the principal direction of the anisotropic hydraulic conductivity tensor. The larger these parameters are, the more dilution is observed in the corresponding flow field. Both parameters could be imposed in the construction of engineered anisotropic porous media, allowing therefore the use of anisotropic fixed-bed chemical reactors to control mixing. This study is also relevant for transient mixing occurring in large-scale anisotropic geologic formations, where similar flow fields may be encountered.

Finally, since transverse dispersion plays a key role to enhance dilution in helical flow fields, a more sophisticated and detailed description of the transverse dispersion coefficient (Chiogna et al. 2010; Scheven 2013) may be needed for practical purposes. Indeed, the characteristic timescale of diffusive processes is, in general, large in comparison with the advective timescale, such that mixing is typically incomplete in pore channels (Rolle et al. 2012; Tartakovsky et al. 2009; deAnna et al. 2014) and Scheidegger's (1961) dispersivity cannot be applied in the dispersion tensor. This may have important implications for reactive solute transport simulations (Chiogna et al. 2012; Ding et al. 2013; Tartakovsky et al. 2009; Chiogna and Bellin 2013) .

Acknowledgments This study was supported by the DFG (Deutsche Forschungsgemeinschaft, CI−26/11 − 1) and Conicyt Chile through Fondecyt Project #11110228. P. Herrera also acknowledges financial support provided by Fondap Project #15090013.

References

Bakker, M., Hemker, K.: Analytic solutions for groundwater whirls in box-shaped, layered anisotropic aquifers. Adv. Water Res. **27**, 1075–1086 (2004)

Bear, J.: Dynamics of Fluids in Porous Media. American Elsevier, New York (1972)

Chiogna, G., Cirpka, O.A., Rolle, M., Bellin, A.: Helical flow in three-dimensional non-stationary anisotropic heterogeneous porous media. Water Resour. Res. **51**, 261–280 (2015)

Chiogna, G., Hochstetler, D.L., Bellin, A., Kitanidis, P.K., Rolle, M.: Mixing, entropy and reactive solute transport. Geophys. Res. Lett. **39**(20), L20405 (2012)

Chiogna, G., Eberhardt, C., Grathwohl, P., Cirpka, O.A., Rolle, M.: Evidence of compound-dependent hydrodynamic and mechanical transverse dispersion by multitracer laboratory experiments. Environ. Sci. Technol. **44**(2), 688–693 (2010)

Chiogna, G., Rolle, M., Bellin, A., Cirpka, O.A.: Helicity and flow topology in three-dimensional anisotropic porous media. Adv. Water Resour. **73**, 134–143 (2014)

Chiogna, G., Bellin, A.: Analytical solution for reactive solute transport considering incomplete mixing within a reference elementary volume. Water Resour. Res. **49**, 2589–2600 (2013)

Cirpka, O.A., Chiogna, G., Rolle, M., Bellin, A.: Transverse mixing in three-dimensional nonstationary anisotropic heterogeneous porous media. Water Resour. Res. **51**(1), 241–260 (2015)

Cleary, P.W., Monaghan, J.J.: Conduction modelling using smoothed particle hydrodynamics. J. Comput. Phys. **148**(1), 227–264 (1999)

de Barros, F., Dentz, M., Koch, J., Nowak, W.: Flow topology and scalar mixing in spatially heterogeneous flow fields. Geophys. Res. Lett. **39**(L08), 404 (2012)

deAnna, P., Dentz, M., Tartakovsky, A., LeBorgne, T.: The filamentary structure of mixing fronts and its control on reaction kinetics in porous media flows. Geophys. Res. Lett. **41**(13), 4586–4593 (2014)

Ding, D., Benson, D.A., Paster, A., Bolster, D.: Modeling bimolecular reactions and transport in porous media via particle tracking. Adv. Water Resour. **53**, 56–65 (2013)

Duplay, R., Sen, P.N.: Influence of local geometry and transition to dispersive regime by mechanical mixing in porous media. Phys. Rev. E **70**(066), 309 (2004)

Falk, M.L., Langer, J.S.: Dynamics of viscoplastic deformation in amorphous solids. Phys. Rev. E **57**(6), 7192–7205 (1998)

Gao, Y., Zang, X., Rama, P., Liu, Y., Chen, R., Ostadi, H., Jiang, K.: Calculating the anisotropic permeability of porous media using the lattice Boltzmann method and X-ray computed tomography. Transp. Porous Med. **92**, 457–472 (2012)

Ginzburg, I., dHumires, D.: Lattice Boltzmann and analytical modeling of flow processes in anisotropic and heterogeneous stratified aquifers. Adv. Water Resour. **30**(11), 2202–2234 (2007)

Guo, P.: Dependency of tortuosity and permeability of porous media on directional distribution of pore voids. Transp. Porous Media **95**(2), 285–303 (2012)
Hemker, K., van den Berg, E., Bakker, M.: Ground water whirls. Ground Water **42**(2), 234–242 (2004)
Hemker, K., Bakker, M.: Analytical solutions for whirling groundwater flow in two-dimensional heterogeneous anisotropic aquifers. Water Resour. Res. **42**(W12), 419 (2006)
Herrera, P.A., Massabó, M., Beckie, R.D.: A meshless method to simulate solute transport in heterogeneous porous media. Adv. Water Resour. **32**(3), 413–429 (2009)
Herrera, P.A., Valocchi, A.J., Beckie, R.D.: A multidimensional streamline-based method to simulate reactive solute transport in heterogeneous porous media. Adv. Water Resour. **33**(7), 711–727 (2010)
Hidalgo, J.J., Fe, J., Cueto-Felgueroso, L., Juanes, R.: Scaling of convective mixing in porous media. Phys. Rev. Lett. **109**(264), 503 (2012)
Higler, A., Krishna, R., Ellenberger, J., Taylor, R.: Counter-current operation of a structured catalytically packed-bed reactor: Liquid phase mixing and mass transfer. Chem. Eng. Sci. **54**, 5145–5152 (1999)
Holm, D.D., Kimura, Y.: Zero-helicity Lagrangian kinematics of three-dimensional advection. Phys. Fluids A **3**(5), 1033–1038 (1991)
Hsieh, P., Neuman, S., Stiles, G., Simpson, E.: Field determination of the three-dimensional hydraulic conductivity tensor of anisotropic media 2. Methodology and application to fractured rocks. Water Resour. Res. **21**(11), 1667–1676 (1985a)
Hsieh, P.A., Neuman, S.P., Stiles, G.K., Simpson, E.S.: Field determination of the three-dimensional hydraulic conductivity tensor of anisotropic media: 2. Methodology and application to fractured rocks. Water Resour. Res. **21**(11), 1667–1676 (1985b)
Hyman, J., Winter, C.: Hyperbolic regions in flows through three-dimensional pore structures. Phys. Rev. E **88**(063), 014 (2013)
Indelman, P., Dagan, G.: Upscaling of permeability of anisotropic heterogeneous formations: 1. The general framework. Water Resour. Res. **29**(4), 917–923 (1993)
Kelley, D.H., Ouellette, N.T.: Separating stretching from folding in fluid mixing. Nat. Phys. **7**, 477–480 (2011)
Kim, J.H., Ochoa, J., Whitaker, S.: Diffusion in anisotropic porous media. Transp. Porous Media **2**(4), 327–356 (1987)
Kitanidis, P.K.: The concept of the dilution index. Water Resour. Res. **30**(7), 2011–2026 (1994)
Koza, Z., Matyka, M., Khalili, A.: Finite-size anisotropy in statistically uniform porous media. Phys. Rev. E **79**(066), 306 (2009)
Le Borgne, T., Dentz, M., Bolster, D., Carrera, J., de Dreuzy, J.R., Davy, P.: Non-Fickian mixing: temporal evolution of the scalar dissipation rate in heterogeneous porous media. Adv. Water Resour. **33**(12), 1468–1475 (2010)
Le Borgne, T., Dentz, M., Villermaux, E.: Stretching, coalescence, and mixing in porous media. Phys. Rev. Lett. **110**(204), 501 (2013)
Le Borgne, T., Dentz, M., Villermaux, E.: The lamellar description of mixing in porous media. J. Fluid Mech. **770**, 458–498 (2015)
Lester, D., Metcalfe, G., Trefry, M.: Is chaotic advection inherent to porous media flow? Phys. Rev. Lett. **111**(174), 101 (2013)
Matyca, M., Koza, Z., Golembiewski, J.: Anisotropy of flow in stochastically generated porous media. Phys. Rev. E **88**(023018) (2013)
Moffatt, H.K.: Helicity and singular structures in fluid dynamics. PNAS **111**(10), 3663–3670 (2014)
Moffatt, H.K., Tsinober, A.: Helicity in laminar and turbulent flow. Ann. Rev. Fluid Mech. **24**(1), 281–312 (1992)
Neuman, S.P., Walter, G.R., Bentley, H.W., Ward, J.J., Gonzalez, D.D.: Determination of horizontal aquifer anisotropy with three wells. Ground Water **22**(1), 66–72 (1984)
Ottino, J.: The Kinematics of Mixing: Stretching, Chaos, and Transport. Cambridge University Press, Cambridge (1989)
Pilotti, M.: Generation of realistic porous media by grains sedimentation. Transp. Porous Media **33**(3), 257–278 (1998)
Rolle, M., Hochstetler, D., Chiogna, G., Kitanidis, P.K., Grathwohl, P.: Experimental investigation and pore-scale modeling interpretation of compound-specific transverse dispersion in porous media. Transp. Porous Media **93**(3), 347–362 (2012)
Rolle, M., Chiogna, G., Hochstetler, D.L., Kitanidis, P.K.: On the importance of diffusion and compound-specific mixing for groundwater transport: an investigation from pore to field scale. J. Contam. Hydrol. **153**, 51–68 (2013)
Scheidegger, A.E.: General theory of dispersion in porous media. J. Geophys. Res. **66**(10), 3273–3278 (1961)
Scheven, U.M.: Pore-scale mixing and transverse dispersivity of randomly packed monodisperse spheres. Phys. Rev. Lett. **110**(214), 504 (2013)

Sposito, G.: Steady groundwater flow as a dynamical system. Water Resour. Res. **20**(8), 2395–2401 (1994)
Sposito, G.: Topological groundwater hydrodynamics. Adv. Water Res. **24**, 793–801 (2001)
Stauffer, F.: Impact of highly permeable sediment units with inclined bedding on solute transport in aquifers. Adv. Water Res. **30**, 2194–2201 (2007)
Stroock, A.D., Dertinger, S.K.W., Ajdari, A., Mezi, I., Stone, H.A., Whitesides, G.M.: Chaotic mixer for microchannels. Science **295**(5555), 647–651 (2002)
Tartakovsky, A.M., Tartakovsky, D.M., Meakin, P.: Stochastic langevin model for flow and transport in porous media. Phys. Rev. Lett. **101**(044), 502 (2008)
Tartakovsky, A., Tartakovsky, G., Scheibe, T.: Effects of incomplete mixing on multicomponent reactive transport. Adv. Water Res. **32**(11), 1674–1679 (2009)
Toussaint, V., Carrire, P., Raynal, F.: A numerical Eulerian approach to mixing by chaotic advection. Phys. Fluids (1994-present) 7(11), 2587–2600 (1995)
van Baten, J., Ellenberger, J., Krishna, : Radial and axial dispersion of the liquid phase within a katapak-s structure: experiments vs. CFD simulations. Chem. Eng. Sci. **56**, 813–821 (2001)
Villermaux, E., Stroock, A.D., Stone, H.A.: Bridging kinematics and concentration content in a chaotic micromixer. Phys. Rev. E **77**(015), 301 (2008)
Ye, Y., Chiogna, G., Cirpka, O.A., Grathwohl, P., Rolle, M.: Experimental evidence of helical flow in porous media. Phys. Rev. Lett. **115**(194), 502 (2015)
Zhu, Y., Fox, P.J.: Simulation of pore-scale dispersion in periodic porous media using smoothed particle hydrodynamics. J. Comput. Phys. **182**(2), 622–645 (2002)